Phys. Med. Biol. **45** (2000) 1665–1682. Printed in the UK PII: S0031-9155(00)07004-4

Visualizing myocardial function using HARP MRI

Nael F Osman and Jerry L Prince†

Center for Imaging Science, Department of Electrical and Computer Engineering, The Johns Hopkins University, Baltimore, MD 21218, USA

E-mail: prince@jhu.edu

Received 16 August 1999

Abstract. Harmonic phase magnetic resonance imaging (HARP) is a new technique for measuring the motion of the left ventricle of the heart. HARP uses magnetic resonance tagging, Fourier filtering and special processing algorithms to calculate key indices of myocardial motion including Eulerian and Lagrangian strain. This paper presents several new methods for visualizing myocardial motion based on HARP. Quantities that are computed and visualized include motion grids, velocity fields, strain rates, pathlines, tracked Eulerian strain, and contraction angle. The computations are fast and fully automated and have the potential for clinical application.

(Some figures in this article appear in colour only in the electronic version; see www.iop.org)

1. Introduction

Determining regional cardiac function is an important objective in the diagnosis of coronary artery disease. Both ischaemia and infarction can be detected and localized through analysis of the regional patterns of motion within the heart. Although echocardiography is the dominant imaging modality for this purpose, magnetic resonance imaging (MRI) has better resolution and lower noise images, allowing more detailed analysis to take place while remaining non-invasive. Further, special magnetic resonance pulse sequences such as tagging (Zerhouni *et al* 1988, Axel and Dougherty 1989) and phase contrast (Pelc *et al* 1991) have been developed to image the detailed motion within the myocardium. The potential to directly image local myocardial function exists with these methods, but noise in phase contrast and processing time in tagging have prevented these approaches from entering into routine clinical use (Budinger *et al* 1998).

Harmonic phase magnetic resonance imaging (HARP) has been recently developed to image the motion of the heart using MR tagging (Osman and Prince 1998a,b, Osman *et al* 2000, 1999a). HARP combines the spatial modulation of magnetization (SPAMM) tagging technique (Axel and Dougherty 1989) with novel image processing algorithms to rapidly measure both Eulerian and Lagrangian strain in the heart. HARP has been compared with a traditional tag processing method and evaluated in both humans (Osman and Prince 1998a,b) and animals (Osman *et al* 1999a, 2000), and it appears to be emerging as the first viable approach for the utilization of MR tagging methods in the clinic. The main advantage of HARP over other methods is its rapid processing time and minimal manual intervention.

† Author to whom correspondence should be addressed at: 105 Barton Hall, Johns Hopkins University, 3400 North Charles Street, Baltimore, MD 21218, USA.

0031-9155/00/061665+18$30.00

In this paper we show new methods to visualize myocardial motion using the HARP framework. In particular, we show how to rapidly compute detailed motion grids, velocity fields, strain rate, angle of maximum contraction and the time evolution of Eulerian strain. These new measurements complement the previously reported algorithms which compute synthetic tags, small displacement fields, Eulerian strain, and Lagrangian strain. All of these computations are fast—together, they can be all calculated in less than 5 min on a typical study—and we show results demonstrating their utility in visualizing abnormal myocardial function. These visualizations provide a rich set of information about myocardial function in the left ventricle. It is strongly felt that these HARP tools will help take MR tagging from the ranks of a valuable scientific research tool into the ranks of a valuable diagnostic clinical tool.

2. Harmonic phase MRI

In this section we review the basics of HARP. At present, details are available only in two conference papers (Osman and Prince 1998a,b), one technical report (Osman *et al* 2000) (submitted separately for journal publication), and one accepted journal paper (Osman *et al* 1999a).

Figure 1(*a*) shows a short-axis, tagged MR image of a canine heart at systole. The left ventricle appears as an annulus at the centre of the image, and the tag lines, which are straight at end-diastole, are bent due to the motion of the heart. The magnitude of the Fourier transform of this image is shown in figure 1(*b*). The spectral peaks that appear in this image arise because of SPAMM tagging, which modulates the underlying image with a truncated cosine series. In fact, it can be shown that the value of a SPAMM-tagged image at image coordinate $\boldsymbol{y}$ and time t can be written as a summation

$$I(\boldsymbol{y}, t) = \sum_{l=-L}^{+L} I_l(\boldsymbol{y}, t) \tag{1}$$

where each complex image $I_l(\boldsymbol{y}, t)$ corresponds to a separate spectral peak (Osman and

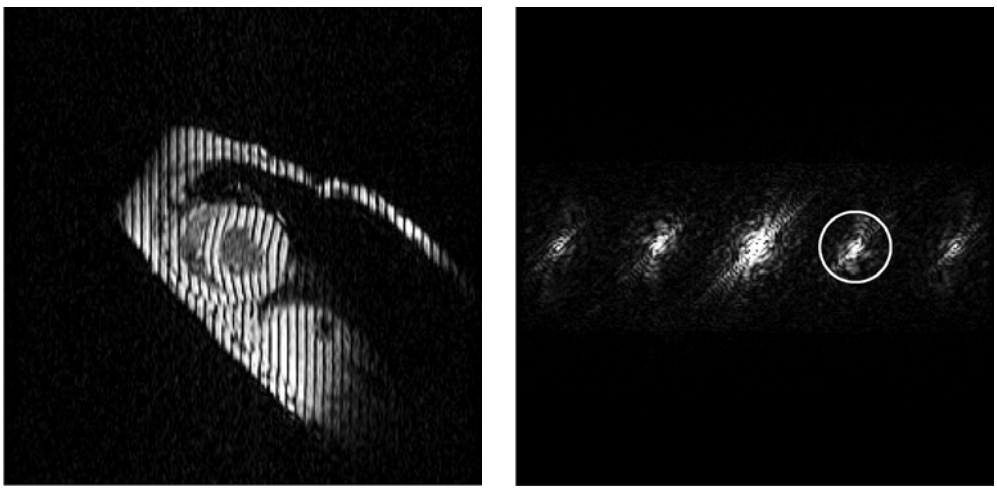

(*a*) (*b*)

Figure 1. (*a*) An MR image with vertical SPAMM tags and (*b*) the magnitude of its Fourier transform.

Prince 1998b). In figure 1(*b*), there are five spectral peaks, so $L = 2$. The spectral peak at the origin ($l = 0$) is the *DC spectral peak* and the other peaks are called the *harmonic spectral peaks*. We refer to the images corresponding to these peaks—that is, the inverse Fourier transforms of the isolated spectral peaks—as the *DC image* and the *harmonic images*.

A harmonic image is a modulated version of the underlying image. Let $\boldsymbol{\omega}$ be the position of the harmonic peak closest to the origin in a standard SPAMM-tagged image. It can be shown that the lth harmonic image is given by

$$I_l(\boldsymbol{y}, t) = D_l(\boldsymbol{y}, t)\, \mathrm{e}^{\,\mathrm{j}l\boldsymbol{\omega}^{\mathrm{T}}\boldsymbol{q}(\boldsymbol{y},t)} \tag{2}$$

where $D_l(\boldsymbol{y}, t)$ is called the *harmonic magnitude image* and $\boldsymbol{q}(\boldsymbol{y}, t)$ is called the *apparent reference map*. The harmonic magnitude image D_l is a real-valued image resembling an untagged MR image. Because tagging is a temporary effect, D_l fades over the cardiac cycle eventually being overwhelmed by noise during diastole. The apparent reference map $\boldsymbol{q}$ gives the apparent position at time 0 (end-diastole) of a material point located at $\boldsymbol{y}$ at time t. The word apparent is used because cardiac motion is three-dimensional, not two-dimensional, so the actual reference position is likely to be out of the image plane. In standard planar tagging, however, the apparent reference position is precisely the projection of the actual reference position onto the image plane. The mathematical relationship between the apparent reference map and a harmonic image given in (2) is the basis of HARP.

From (2) we see that the motion, described by $\boldsymbol{q}(\boldsymbol{y}, t)$, phase-modulates the underlying image. This causes a spreading of the energy around the spectral peak, the extent of which depends on both the magnitude of $l\boldsymbol{\omega}$ and the magnitude of the motion. In short-axis images with tag planes parallel to the long axis, the spreading is reasonably localized around $l\boldsymbol{\omega}$, and it is possible to design a bandpass filter whose elliptical bandpass region isolates a single spectral peak including most of the effects of phase modulation.

In our work to date we have concentrated on the use of just two spectral peaks, a first-order harmonic from each of the horizontal and vertical tagged images. Despite the abuse of notation, we will refer to these two harmonic images as $I_l(\boldsymbol{y}, t)$, $l = 1, 2$. These images are represented mathematically by

$$I_l(\boldsymbol{y}, t) = D_l(\boldsymbol{y}, t)\, \mathrm{e}^{\,\mathrm{j}\phi_l(\boldsymbol{y},t)} \tag{3}$$

where

$$\phi_l(\boldsymbol{y}, t) = \boldsymbol{\omega}_l^{\mathrm{T}}\boldsymbol{q}(\boldsymbol{y}, t) \tag{4}$$

and $\boldsymbol{\omega}_l$, $l = 1, 2$, represent the positions of the harmonic peaks closest to the origin in the vertical and horizontal tagging directions, respectively. We call ϕ_l a *harmonic phase image*. It is convenient to write the two harmonic phase images arising from vertical and horizontal tagging using the vector $\boldsymbol{\phi}(\boldsymbol{y}, t) \stackrel{\triangle}{=} [\phi_1(\boldsymbol{y}, t)\ \phi_2(\boldsymbol{y}, t)]^{\mathrm{T}}$. This harmonic phase vector is related to the motion by the compact matrix expression

$$\boldsymbol{\phi}(\boldsymbol{y}, t) = \Omega^{\mathrm{T}}\boldsymbol{q}(\boldsymbol{y}, t) \tag{5}$$

where

$$\Omega \stackrel{\triangle}{=} [\boldsymbol{\omega}_1\ \boldsymbol{\omega}_2]. \tag{6}$$

If harmonic phase images could be computed then the reference map could be directly computed by inverting Ω. Unfortunately, harmonic phase images can only be computed using phase unwrapping, a difficult and generally impractical procedure. Instead, we must use the wrapped versions of harmonic phase images, which can be directly computed from harmonic

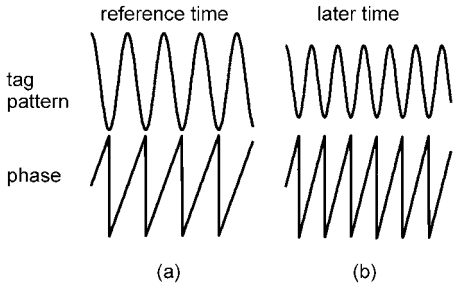

Figure 2. The principle of HARP MR image processing. A sinusoidal tag pattern and its phase at the reference time is shown in (*a*). At a later time, as shown in (*b*), the tag pattern has decayed in amplitude from fading and become higher frequency because of 'tissue' compression. The phase in (*b*) is unchanged in amplitude but has a larger slope.

images using the arctangent of the ratio of the imaginary to real parts. The relationship between the wrapped harmonic phase vector $\boldsymbol{a}$ and ϕ is

$$\boldsymbol{a} = \mathcal{W}(\phi) \tag{7}$$

where the wrapping function $\mathcal{W}$ is given by

$$\mathcal{W}(\phi) = \text{mod}(\phi + \pi, 2\pi) - \pi. \tag{8}$$

The essential difficulty in harmonic phase imaging is dealing with the effects of wrapping.

The basic idea behind HARP methods can be illustrated using a simple one-dimensional example, as shown in figure 2. Figure 2(*a*) depicts a sinusoidal tag pattern and its corresponding (wrapped) phase and figure 2(*b*) depicts the pattern and phase of the same region of tissue at a later time. The effect of a tissue compression and tag fading has caused the tag pattern frequency to increase and its amplitude to decrease. The effect on the phase of the pattern is to increase its slope, but its amplitude is unaffected. We see immediately that the slope of the phase is related to the underlying tissue strain. Local phase unwrapping is easily employed to estimate the correct slope at the points of phase discontinuity. We note that this measure gives Eulerian strain since it represents the local tissue strain at a spatial coordinate rather than a material coordinate. We also see that the value of the phase can be used to track points. Although there is potential ambiguity since the phase values are not unique, if the motion is small enough the points can be uniquely associated. Once tracking is accomplished, Lagrangian strain can be computed by tracking material points and calculating their patterns of motion.

In previous work, we have developed algorithms to rapidly estimate Eulerian strain (Osman *et al* 2000) and to track points for computation of Lagrangian strain (Osman *et al* 1999a). These algorithms use pairs of horizontal and vertical tagged images and their corresponding harmonic phase vectors to estimate two-dimensional motion. Eulerian strain can be directly computed and visualized as radial or circumferential strain at any time within the cardiac cycle and time sequences can be built up to show movies of Eulerian strain. CINE tagged MR images are used to track the points through time (so-called CINE HARP) so that incremental motion is small enough to avoid phase ambiguities. The results of point tracking can be used to compute and plot the course of Lagrangian strain. The LV can be divided into octants and average Lagrangian strain computed and plotted over the course of time. These methods were developed and validated using simulated, animal and human data. In the following sections, we extend the capabilities of HARP by developing several new methods to calculate and visualize heart motion.

3. Methods

3.1. Motion grids

Simple visualization of tag lines has potential for use in diagnosis. It is possible to recognize abnormal patterns of motion due to infarction, abnormal electrical excitation, and ischaemia. Currently, it is most common to visualize the horizontal and vertical tagged images separately or to visualize grid patterns generated by two-dimensional tagging or the superposition of vertical and horizontal tagged images (e.g. the multiplication of figure 1(*a*) with its horizontally tagged counterpart). The resolution of this result is limited to the resolution of the tag lines, however, and this is limited by the image resolution. As described in Osman and Prince (1998b) and Osman *et al* (2000), HARP offers the capability to 'synthesize' artificial tag lines to arbitrary resolution. In this section, we describe an automatic method to generate motion grids using the synthetic tag concept. Motion grids provide a visual summary of LV motion using a deforming grid pattern.

Consider a single harmonic phase image $\phi_l(\boldsymbol{y}, t)$. Since harmonic phase is a material property (moves with the tissue), the set of points having a given target harmonic phase ϕ at a given time —an isocontour at level ϕ—is a curve. When the wrapped image $\boldsymbol{a}_l(\boldsymbol{y}, t)$ is used, the target harmonic phase $\boldsymbol{a}$ must be chosen in the range of the arctangent operator $[-\pi, +\pi)$ and, in principle, one curve per tag period should be selected per target phase. The presence of wrapping discontinuities, however, causes an additional curve to be selected at the phase discontinuity (see figure 2), an undesirable effect.

A simple fix to this problem is to take the absolute value of the (wrapped) harmonic phase image $|a_l|$. Then if the target phase for an isocontour algorithm is $\pi/2$, two curves per period will be produced, evenly spaced at end-diastole, and there will be no additional curve generated at the discontinuities (because the discontinuities are removed by the absolute value operator). This procedure can be extended to generate more curves per tag period. The second stage would subtract $\pi/2$ from $|a_l|$, take another absolute value, and choose $\pi/4$ as the isocontour threshold. This procedure can be repeated again and again to get what amounts to arbitrarily close tag lines which are evenly spaced at end-diastole. To generate motion grids this algorithm is applied to both the horizontal and vertical harmonic phase images and the resulting isocontours are superposed.

3.2. Velocity fields

Phase contrast MRI uses special pulse sequences to compute velocity fields which can then be used for a variety of purposes including visualization (Pelc *et al* 1991, 1995, Constable *et al* 1994). HARP tracking can be used to produce such fields by computing the apparent displacement between two successive images in a CINE tagged sequence. Applying HARP tracking to all the points in an image, however, is a computationally intensive task, and perhaps it is unnecessary if visualization is the only goal. In this section we present a fast algorithm for the computation of velocity fields in CINE tagged sequences using an optical flow method. Because the harmonic phase of a point does not change with time, optical flow can be applied to the harmonic phase images, rather than the intensity images (as in conventional optical flow). This use of harmonic phase images is similar to the phase-based optical flow method described in Fleet and Jepson (1990).

Since the harmonic phase of a material point remains constant as it moves, we have

$$\frac{\mathrm{d}\phi}{\mathrm{d}t} = 0$$

which can be rewritten using the chain rule as

$$\nabla\phi(\boldsymbol{y}, t)\boldsymbol{v}(\boldsymbol{y}, t) + \frac{\partial\phi}{\partial t} = 0$$

where ∇ is the gradient with respect to $\boldsymbol{y}$ and $\boldsymbol{v}(\boldsymbol{y}, t)$ is the *velocity field* at time t. Solving for $\boldsymbol{v}$ yields

$$\boldsymbol{v}(\boldsymbol{y}, t) = -[\nabla\phi(\boldsymbol{y}, t)]^{-1}\frac{\partial\phi}{\partial t}. \tag{9}$$

We note that it can be shown that the matrix $\nabla\phi$ is always invertible. The actual harmonic phase vector ϕ is not easily calculated, however, so another approach must be taken to compute the quantities on the right-hand side of (9).

As in the calculation of Eulerian strain, the spatial derivative of ϕ can be readily calculated since it is the same as the spatial derivative of $\boldsymbol{a}$ except at the points of discontinuities of $\boldsymbol{a}$. It can be shown that (Osman *et al* 2000)

$$\nabla\phi = \nabla^*\boldsymbol{a} \triangleq \begin{bmatrix} \nabla^* a_1 \\ \nabla^* a_2 \end{bmatrix} \tag{10}$$

where

$$\nabla^* a_l \equiv \begin{cases} \nabla a_l & \|\nabla a_l\| \leqslant \|\nabla\mathcal{W}(a_l + \pi)\| \\ \nabla\mathcal{W}(a_l + \pi) & \text{otherwise} \end{cases} \tag{11}$$

for $l = 1, 2$. Finite differences are used to compute the elements of the gradient operators.

The time derivative of ϕ is computed using finite differences of $\boldsymbol{a}$ in successive frames of the CINE sequence. It turns out that the effects of wrapping can be entirely removed by rewrapping this result, and the correct finite difference approximation is given by

$$\frac{\partial\phi}{\partial t}(\boldsymbol{y}, t_n) \approx \frac{1}{\Delta t}\mathcal{W}[\boldsymbol{a}(\boldsymbol{y}, t_{n+1}) - \boldsymbol{a}(\boldsymbol{y}, t_n)] \tag{12}$$

where Δt is the time separation between the images at t_n and t_{n+1}. This expression is valid provided that $|\phi(\boldsymbol{y}, t_{n+1}) - \phi(\boldsymbol{y}, t_n)| < \pi$, a small motion assumption, which is guaranteed if Δt is sufficiently small. Putting these elements together yields an expression for the estimated velocity field

$$\boldsymbol{v}(\boldsymbol{y}, t_n) = -\frac{1}{\Delta t}\nabla^*\boldsymbol{a}^{-1}(\boldsymbol{y}, t_{n+1})\mathcal{W}[\boldsymbol{a}(\boldsymbol{y}, t_{n+1}) - \boldsymbol{a}(\boldsymbol{y}, t_n)] \tag{13}$$

which can be computed rapidly using two harmonic phase images and two successive time instants in a CINE acquisition.

3.3. Strain rate

Strain rate, the change in strain per unit time, has also proven useful in assessing cardiac function (Beache *et al* 1995). It has been both directly imaged using the MR scanner (Wedeen 1992) and calculated from phase contrast velocity fields (Wedeen *et al* 1995). Here, we use its fundamental relationship with velocity to calculate strain rate from HARP velocity fields.

We use the 2×2 strain rate tensor

$$S(\boldsymbol{y}, t) = \frac{1}{2}[\nabla\boldsymbol{v}(\boldsymbol{y}, t) + \nabla^{\mathrm{T}}\boldsymbol{v}(\boldsymbol{y}, t)] \tag{14}$$

as defined in Wedeen (1992). To visualize this tensor, we display its radial and circumferential components. We first define the centre of the LV, which can be done manually or automatically through the scanner prescription used to generate the short-axis images. The radial direction

field $\boldsymbol{e}_R(\boldsymbol{y}, t)$ and the circumferential direction field $\boldsymbol{e}_C(\boldsymbol{y}, t)$ are automatically determined. The radial and circumferential strain rates are then given, respectively, by

$$S_{RR}(\boldsymbol{y}, t) = \boldsymbol{e}_R(\boldsymbol{y}, t)^{\mathrm{T}} S(\boldsymbol{y}, t) \boldsymbol{e}_R(\boldsymbol{y}, t) \tag{15}$$

$$S_{CC}(\boldsymbol{y}, t) = \boldsymbol{e}_C(\boldsymbol{y}, t)^{\mathrm{T}} S(\boldsymbol{y}, t) \boldsymbol{e}_C(\boldsymbol{y}, t). \tag{16}$$

3.4. Contraction angle

Eulerian strain in two dimensions is related to the change in tag frequency, which is in turn reflected by a change in slope of harmonic phase. In Osman and Prince (1998b) and Osman *et al* (2000), we showed how to calculate circumferential and radial strain using gradients of harmonic phase images and the reference directions $\boldsymbol{e}_R$ and $\boldsymbol{e}_C$. Here, we describe how to calculate a two-dimensional strain tensor from which the direction of maximum contraction, or the *contraction angle*, can be calculated and visualized.

The left Cauchy–Green strain tensor is given by Gurtin (1981)

$$B \triangleq [\nabla \boldsymbol{q}]^{-1} [\nabla \boldsymbol{q}]^{-\mathrm{T}}. \tag{17}$$

Using (5) and (10), we find that $\nabla \boldsymbol{q} = \Omega^{-\mathrm{T}} \nabla^* \boldsymbol{a}$; hence

$$B = [\nabla^* \boldsymbol{a}]^{-1} \Omega^{\mathrm{T}} \Omega [\nabla^* \boldsymbol{a}]^{-\mathrm{T}}. \tag{18}$$

The square root of the eigenvalues of B gives the maximum shortening and thickening at any location. The corresponding eigenvectors, which are orthogonal to each other, represent the principal strain directions—the directions of maximum shortening and maximum thickening.

The orientation of maximum thickening has been shown to be a sensitive indicator of LV myocardial performance (Marcus *et al* 1997). The angle β is defined to be the angle between the direction of maximum thickening and the radial direction. Letting $\boldsymbol{v}_1$ denote the (unit) eigenvector of B corresponding to its largest eigenvalue, this angle is given by

$$\beta = \arccos(\boldsymbol{v}_1 \cdot \boldsymbol{e}_R). \tag{19}$$

The contraction angle β is small (around 12 degrees) at end-systole in normal myocardium, but is typically much larger when there are local motion abnormalities (Marcus *et al* 1997).

3.5. Pathlines

Motion grids reveal the pattern of motion by displaying curves of constant harmonic phase over time. The intersection of horizontal and vertical lines are points, which can be followed as (apparent 2D) material points over time. There is nothing special about the actual HARP values these points possess, however. Any point in the image having any two HARP values can be tracked through a CINE sequence, and we reported a robust method to do this in Osman *et al* (1999a), which we called *HARP tracking*. The result is an estimate of the motion map $\boldsymbol{y}(\boldsymbol{q}, t_n)$ for $n = 1, \ldots, N$.

We used the results of tracking to describe Lagrangian strain, which is determined by the change in size and shape of collections of material points after deformation. A very simple alternative use for tracking, however, is in visualization of myocardial motion via pathlines, which are the trajectories that points take over time. Mathematically, the pathline of material point $\boldsymbol{q}$ is given by the set

$$\mathcal{P}(\boldsymbol{q}) = \{\boldsymbol{y}(\boldsymbol{q}, t) \mid t > 0\} \tag{20}$$

which we observe at the discrete times $t = t_n$, $n = 1, \ldots, N$. Overall motion of the LV myocardium can be assessed by simultaneously displaying the pathlines of a collection of material points within the LV wall.

3.6. Movies of Lagrangian strain

Using HARP tracking, Lagrangian strain can be computed. In previous work, we computed Lagrangian strain on a circular coordinate system and plotted the time evolution of circumferential and radial strain for different octants within the left ventricle. Here, we consider the rectangular coordinate system of the image at the reference time and calculate movies of changing Lagrangian strain of myocardial material points.

Given $\boldsymbol{y}(\boldsymbol{q}, t)$ for all points within the myocardium at the reference time, we use spatial differences to compute the deformation gradient tensor $\nabla_q \boldsymbol{y}(\boldsymbol{q}, t)$ where ∇_q represents the gradient with respect to $\boldsymbol{q}$. The right Cauchy–Green strain tensor is given by $C(\boldsymbol{q}, t) = \nabla_q \boldsymbol{y}(\boldsymbol{q}, t)^{\mathrm{T}} \nabla_q \boldsymbol{y}(\boldsymbol{q}, t)$. The radial component of strain is then computed using $\boldsymbol{e}_R^{\mathrm{T}} C \boldsymbol{e}_R - 1$, and the circumferential component of strain is computed using $\boldsymbol{e}_C^{\mathrm{T}} C \boldsymbol{e}_C - 1$, where $\boldsymbol{e}_R$ and $\boldsymbol{e}_C$ the radial and circumferential unit vectors at the reference time ($t = 0$).

These strains can be visualized as a movie in which the geometry remains fixed and the image grey scale depicts strain. This represents a fixed-anatomy visual display of function. One potential advantage of this type of visualization over a movie of Eulerian strain is that here the strain is calculated with respect to fixed radial and circumferential directions, rather than directions that change with time.

3.7. Time evolution of Eulerian strain

In previous work, we have plotted the time evolution of Lagrangian strain averaged over octants of the left ventricle (Osman *et al* 1999b). We have also shown time sequences of Eulerian strain images (Osman and Prince 1998b, Osman *et al* 2000). Now that in the previous section we have proposed movies of Lagrangian strain, it is natural to 'fill in the matrix' with plots of the time evolution of Eulerian strain.

Eulerian strain and Lagrangian strain are the same quantity except that they usually have different frames of reference. For example, in our work Lagrangian strain is typically referenced to the first imaged frame immediately after end-diastole and the radial and circumferential directions are referenced to either the same frame or the systolic frame. On the other hand, Eulerian strain is referenced to the moment that the tags were applied, typically end-diastole, which is usually 15–30 ms before the first imaged frame. Also, the radial and circumferential directions evolve temporally according to a spatial coordinate system with a shifting (but not rotating) origin.

With tracking, it is possible to display *any* calculated quantity, material or spatial, in a Lagrangian sense—that is, by following the material point. Therefore, to assess the difference between calculated Lagrangian and Eulerian strains, we propose calculating both strains and plotting their values averaged over octants identified within the first imaged frame. The Eulerian strain values are determined for these selected points by tracking their positions and interpolating their radial and circumferential Eulerian strains from the spatial calculations described in Osman and Prince (1998b). The results are plots of the temporal evolution of both Lagrangian and Eulerian strain by LV octant.

4. Experiments

To demonstrate the capabilities of HARP, a set of tagged images of an ectopically paced canine heart were used. The strain that is generated from LV ectopic pacing shows very rapid changes in both time and space. Hence, the strain fields generated are some of the most challenging for the existing strain modelling methods. These data were previously used in a study of cardiac

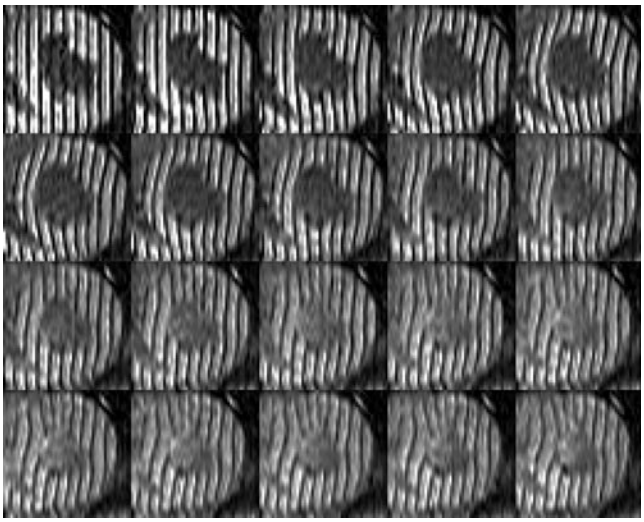

(*a*)

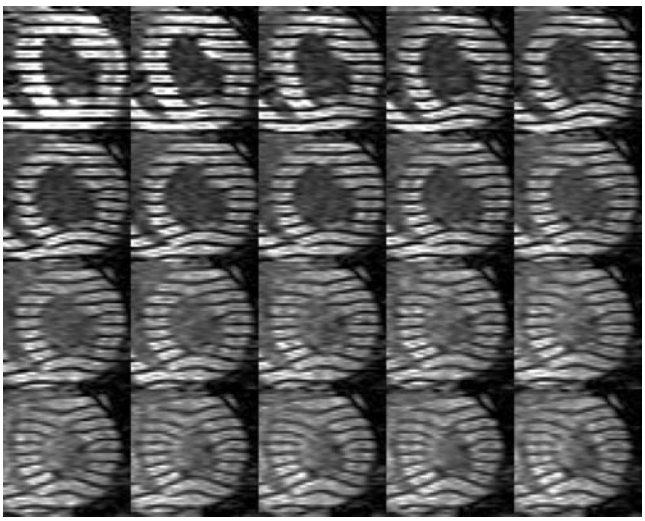

(*b*)

Figure 3. Two short-axis image sequences of a paced canine heart showing (*a*) vertical tags and (*b*) horizontal tags. The sequence is ordered from end-diastole at the top left proceeding left to right then top to bottom to end-systole at bottom right.

motion under ectopically paced activation using tagged MR imaging and previously proposed analysis techniques. A complete description of the experimental protocol and their results are given in McVeigh *et al* (1998). Although our results yield only apparent motion and strain on a single cross-section rather than giving a complete 3D description, the results we obtain here are very nearly the same as those in McVeigh *et al* (1998) and are generated in only a fraction of the time.

A pacing lead was sewn onto the epicardial surface of left ventricular basal free wall of a canine heart. MR imaging was performed on a standard 1.5 T scanner with software release 4.7 (General Electric Medical Systems, Milwaukee, WI). A 6 ms SPAMM pulse sequence was

used to produce a tag pattern in the myocardium comprising parallel plane saturation bands separated by 5.5 mm in the image plane. The tagging pulse sequence was triggered with a signal from the pacer, and the imaging sequence started 3 ms after the tagging pulses were completed. The image scanning parameters were: TR = 6.5 ms, TE = 2.1 ms, readout bandwidth = ±32 kHz, 320 mm field of view, 256 × 96 acquisition matrix, fractional echo, two readouts per movie frame and 6 mm slice thickness.

Two sequences of 20 tagged MR short-axis images, one with horizontal tags and the other with vertical tags, were acquired at 14 ms intervals during systole. The images were acquired during breath-hold periods with segmented k-space acquisition, and in this paper we use those acquired in a basal plane, near the location of the pacing lead. Figure 3 shows the resulting images cropped to a region of interest around the LV to show vertical and horizontal tags in panels (*a*) and (*b*) respectively. Strong early contraction can be seen near the pacing lead on the inferior lateral wall at about 5 o'clock. The septal wall is seen to bow outward in frames 4–8, an abnormal motion called *pre-stretching* caused by a delay in the electrical activation signal to the septal region. After this, the entire LV myocardium experiences continued contraction throughout systole in nearly normal fashion.

HARP images were computed from the vertical tagged image sequence using the bandpass filter depicted in figure 1(*b*); a 90 degree rotated version of this filter was used to compute the horizontal HARP images. All images in figure 3 were filtered, and the resulting vertical and horizontal HARP images were used in all subsequent motion visualization calculations.

5. Results and discussion

5.1. Motion grids

Figure 4 shows a sequence of motion grids computed using two isocontours per period. The grid is superimposed on a crude segmentation of the myocardium created using HARP magnitude images (cf Osman and Prince 1998b, Osman *et al* 2000). It is observed that the overall pattern

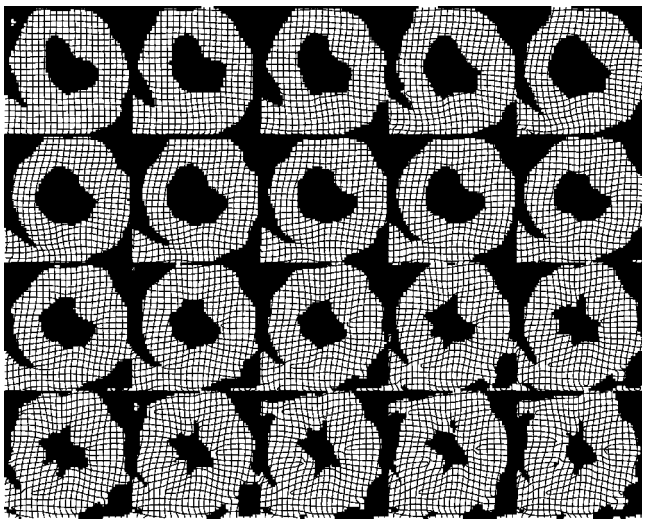

Figure 4. A sequence of motion grids ordered the same way as in figure 3.

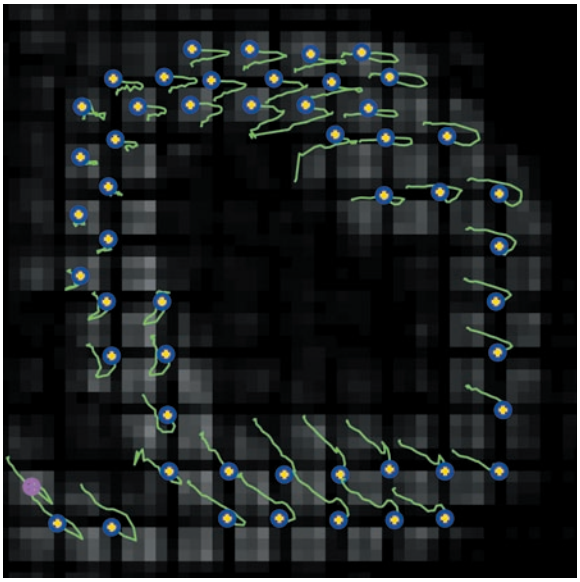

Figure 5. The pathlines of manually selected points (bold circles).

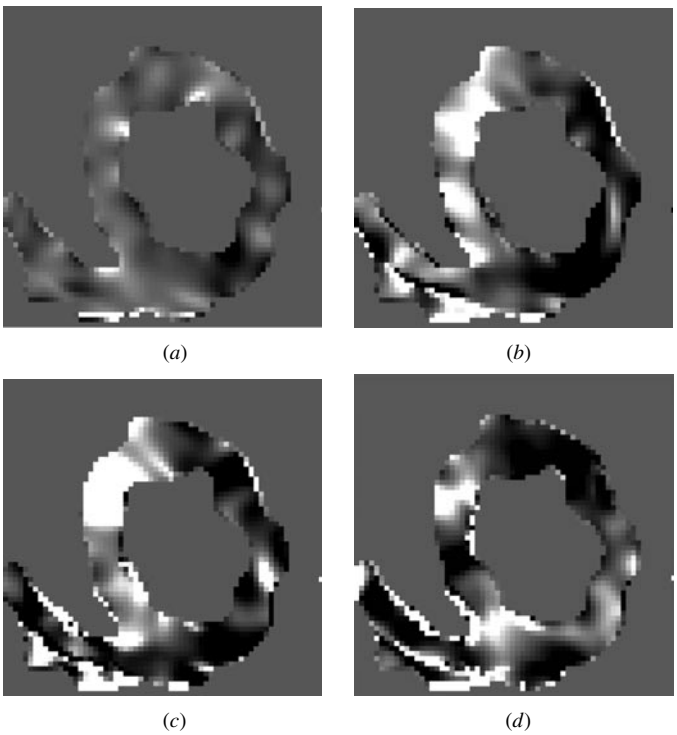

Figure 6. Selected frames from a movie showing Lagrangian circumferential strain. The time frames are (*a*) 2, (*b*) 4, (*c*) 6 and (*d*) 12. Dark regions indicate shortening while light regions indicate stretching.

of contraction evident in figure 3 is still present, but the apparent resolution has increased by a factor of two.

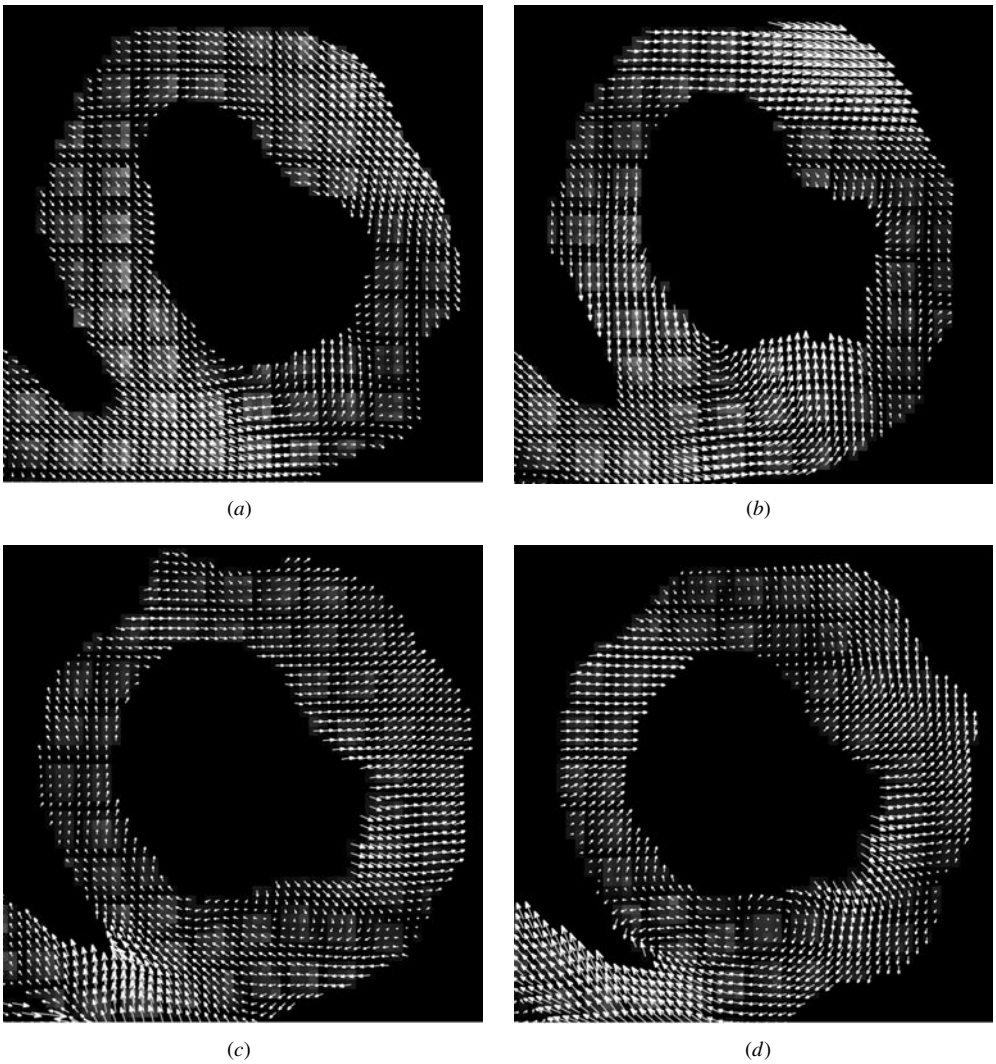

(*a*) (*b*)

(*c*) (*d*)

Figure 7. Velocity fields computed between times (*a*) 1–2, (*b*) 2–3, (*c*) 5–6 and (*d*) 6–7.

It cannot be argued that HARP provides *more* information about motion than the original images—after all, HARP images result from the removal of information through filtering and subsequent novel processing and presentation of these data. Therefore, motion grids represent a type of *interpolation* between tag data, and they are generated entirely automatically. For visualization of the data motion grids may represent an improvement over simple visualization of the original data.

5.2. Motion trajectories

Figure 5 shows a collection of points and their pathlines calculated by CINE HARP. The underlying image was created by multiplying the horizontal and vertical tagged images at the first time frame to show a tagging grid. The points were selected manually in order to give a broad view of the different types of point motion in this paced canine heart.

Figure 8. A circular grid superposed on the left ventricular wall. There are 48 points, 16 on each circle, characterizing the sub-endocardium, midwall and sub-epicardium using six points per octant.

Several observations can be made from this result. First, since several points are located in the right ventricle, this experiment demonstrates the ability for HARP to measure right ventricular motion. Second, the motion of the points within the free wall are larger than those of the septum and the free wall seems to move toward the septum during systole. This confirms a common observation. Finally, the points at approximately 1 o'clock and 8 o'clock on the LV wall begin their pathline by moving away from the 10 o'clock position. This is an indication of the abnormal motion caused by the pacemaker, which is located at approximately 5 o'clock. What happens is that initially the electrical activation is limited to the myocardium near the pacemaker. Muscle on the opposing wall is actually stretched until the electrical signal arrives.

5.2.1. Movies of Lagrangian strain. A segmentation mask roughly indicating the myocardium was calculated using the HARP magnitude image from the first frame. For each point in the myocardium, a time sequence of Lagrangian circumferential strain was computed using CINE HARP. Figure 6 shown images of this strain at four different times during systole. We note that the strain is presented in the reference coordinate system, which explains the rigidity of the geometry.

Several observations can be made from this result. In figure 6(*a*), the second time frame, we observe a darker region at the 5 o'clock position. This represents an early contraction at the site of the pacing lead. This contraction is larger in figure 6(*b*) and now stretching is observed at the 10 o'clock position. In figure 6(*c*), the sixth time frame, the early contraction is less apparent, while the prestretching is very strong. Figure 6(*d*) shows the twelfth time frame where other regions (1 and 8 o'clock) are undergoing some contraction.

5.3. Velocity fields

Figure 7 shows four velocity fields computed between different time frames in the cine sequence. In (*a*) we see a very compelling picture of an abnormal pattern of excitation. The velocity vectors at 8 and 2 o'clock are pointing circumferentially toward the pacing site, and the vectors at 10 o'clock are clearly pulling inward but separating circumferentially. Meanwhile, at the pacing site, the vectors are separating radially, indicating the thickening of the muscle, i.e. normal contraction. In (*b*), this general pattern continues, but evidence of radial thickening is spreading from the site of excitation. In (*c*) and (*d*), the velocity vectors show a reversal

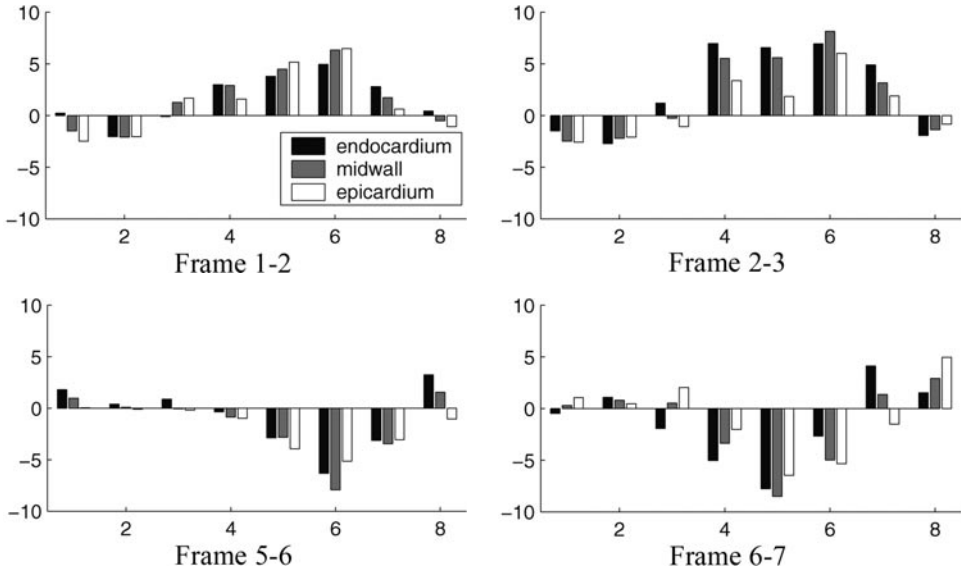

(*a*)

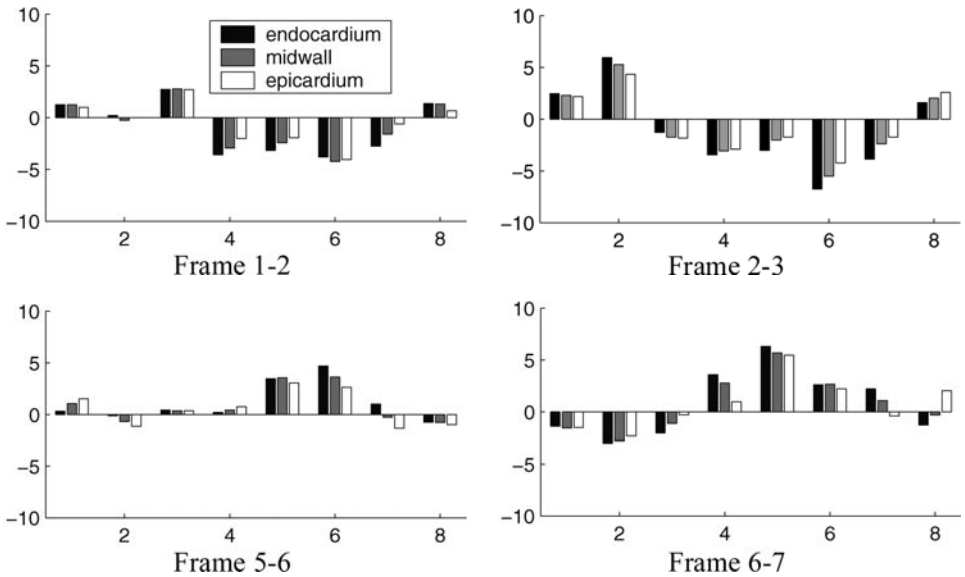

(*b*)

Figure 9. (*a*) The radial strain rate and (*b*) the circumferential strain rate for various time frames and different radial wall layers. The vertical axes indicate percentage of variation during the interval between the two time frames. Negative values indicate shortening while positive values indicate stretching.

of direction as the muscle opposite the pacing site is activated. In this case, it is not so easy to discern local strain, as the overall magnitude of the vectors is quite large in most regions. An interesting rotational effect is observed in (*d*) at 6 and 12 o'clock. These represent the locations where the right ventricular wall joins the left, but otherwise it is not known why this effect should be present.

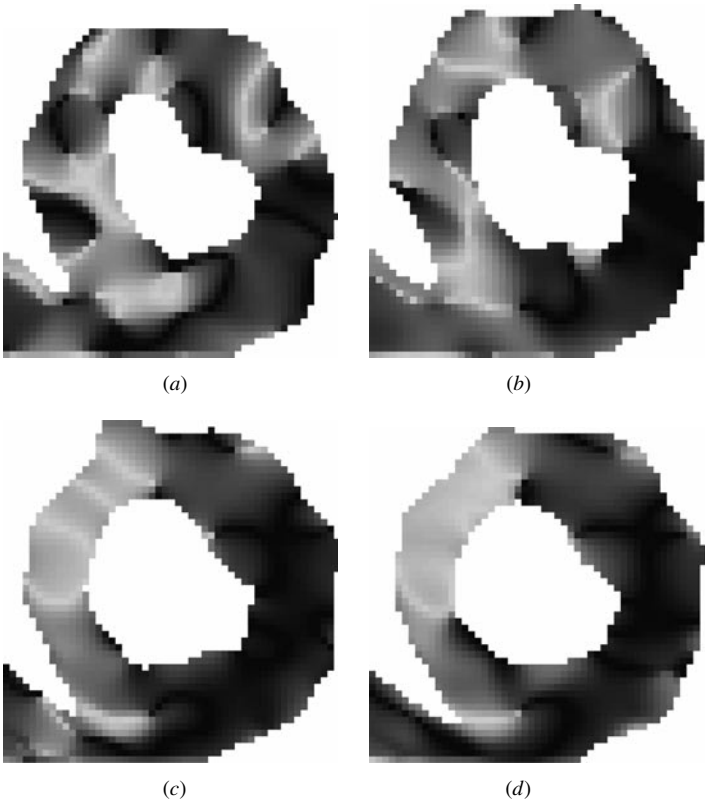

Figure 10. Images of contraction angle for time frames (*a*) 1, (*b*) 2, (*c*) 5 and (*d*) 6. Dark indicates smaller angles, while bright indicates larger angles.

Visualization of myocardial velocity with this level of clarity and resolution is not possible with any other technique to the knowledge of the authors. The possibilities for further scientific and medical research using this approach are wide open at present.

5.4. Strain rate

Because of the spatial differentiation required to compute strain rate, these make very noisy images. Another way to visualize—indeed, to quantify—strain rate is to average over octants and display these averaged results. Accordingly, we averaged the strain rate over the octants depicted in figure 8 in three radial bands: mid-wall, sub-endocardial, and sub-epicardial. The averaged strain rate results are shown in figure 9.

In figure 9(*a*), the early large positive radial strain rate in octant 6 coincides with the location of the pacing lead and indicates that a myocardial thickening is taking place. Although difficult to discern from the velocity plots themselves, the opposite wall (octant 2) is showing a slight negative radial strain rate, indicating a myocardial thinning. At the later times, the sign of the strain rate reverses. This indicates that the opposite wall is starting to contract, while the wall nearest the pacer is starting to relax. We speculate that this is caused by a drop in tension due to muscle fatigue which is in turn caused by the prolonged stimulation around the pacing lead.

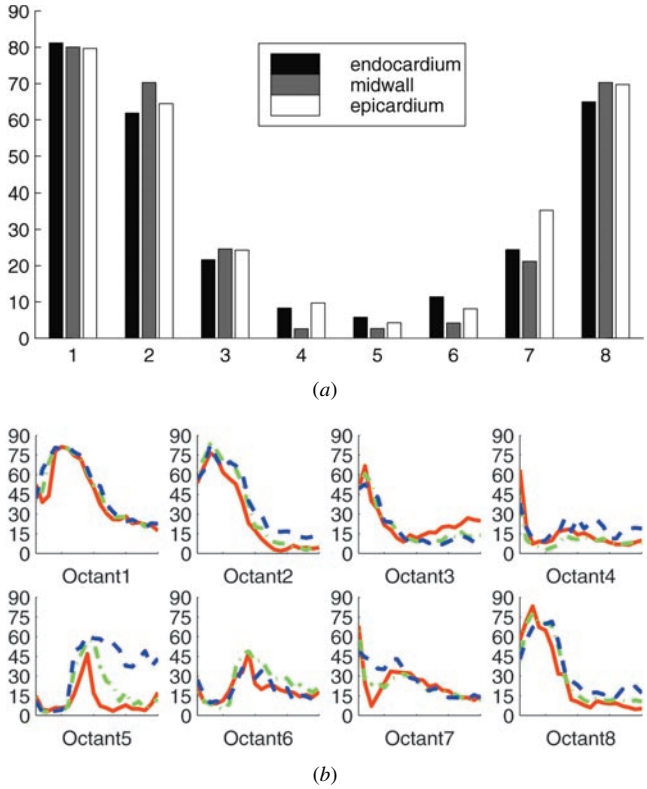

Figure 11. The plot in (*a*) shows the contraction angle distribution at the fifth time frame for the different octants of the LV. Panel (*b*) shows the time evolution of the contraction angles in different octants. The solid, dashed-dotted and dashed curves represent the sub-endocardium, midwall and sub-epicardium respectively.

The circumferential strain rate, shown in figure 9(*b*), agrees point-by-point with the above interpretation. The contrasting levels of strain rate, either radial or circumferential, is indicative of abnormal motion, which in this case is due to the ectopic pacing. In normal motion, a more homogeneous activity would be observed.

5.5. Contraction angle

The contraction angle was computed for all time frames, four of which are displayed in figure 10. The time frames are selected to be the first time frame of the pairs used to compute velocity in figure 7. In early contraction, the motion is very small over most of the LV wall, so there is a fairly random pattern of angle. At later times, however, there is a striking differentiation between muscle strongly contracting near the pacing lead (5 o'clock) and that which is stretching on the opposite wall.

To demonstrate the differences in contraction angle, in figure 11(*a*) we plotted the average contraction angle at the fifth time frame over the octants of figure 8. The large difference between the angles shows the sensitivity of the contraction angle to the abnormality of the motion. The full time evolution of contraction angle is shown in figure 11(*b*). It is important to note that the contraction angle in octant 2 decreases quite dramatically toward systole; this is when this muscle has been activated and is contracting properly. One can speculate that

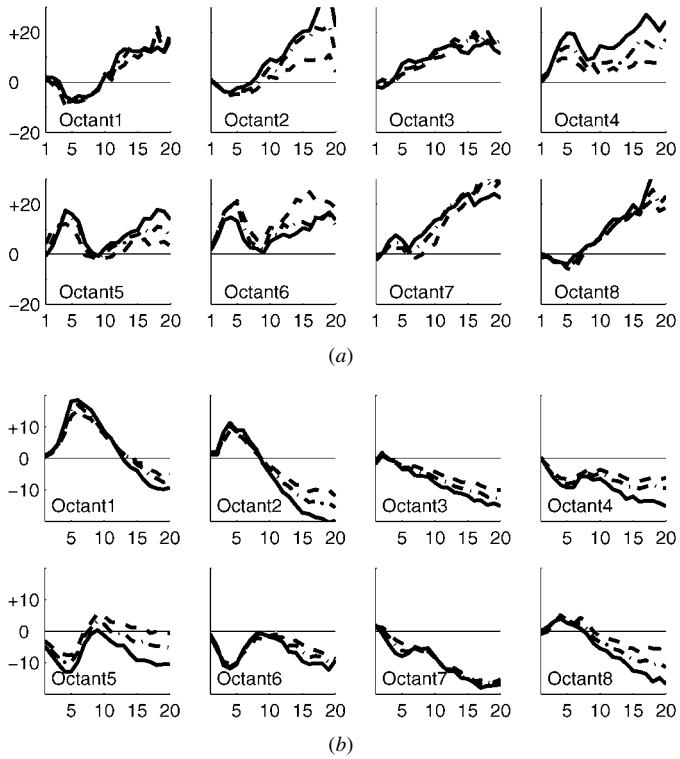

Figure 12. Time evolution of (*a*) radial and (*b*) circumferential Eulerian strain. The solid, dashed-dotted and dashed curves represent the sub-endocardium, midwall and sub-epicardium respectively.

infarcts and ischaemic tissues would have their own contraction angle 'signatures' that could be recognized for diagnosis.

5.6. Time evolution of Eulerian strain

Figures 12(*a*) and 12(*b*) show the time evolution of radial and circumferential Eulerian strains, respectively, within the octants depicted in figure 8. These plots are very similar to the Lagrangian strain results reported in Osman *et al* (1999a). Early contraction around octant 5 is evident in both the radial and circumferential strains. This contrasts nicely with early stretching evident around octant 1. One feature not readily apparent from the images of Eulerian and Lagrangian strain is the loss of strain around octant 5 at about the tenth time frame. This can be explained by the muscle fatigue around the pacing site due to the early contraction.

There is one important difference between these Eulerian strain plots and the Lagrangian strain plots. This difference is evident in the circumferential strain of octant 5 (figure 12(*b*)), where the strain values at the first time frame are *not* zero, as they are in the Lagrangian strain plots in Osman *et al* (1999a). This is because the reference time for the Eulerian strains is the moment the tags were placed in the tissue (end-diastole), whereas the reference time of the Lagrangian strains is, by necessity, the first imaged time. Since the first imaging time frame is about 10 ms after end-diastole, the non-zero Eulerian strain indicates (and localizes) contraction that has already taken place as the consequence of the ectopic pacing activation.

6. Conclusion

We have presented new methods for visualizing the motion of the heart using tagged MR images. These methods are based on HARP, harmonic phase MRI, which in turn uses the unique spectral properties of SPAMM tagging to calculate various motion quantities. In particular, we developed motion grids, velocity fields, strain rates, pathlines, tracked Eulerian strain and contraction angle. These methods, demonstrated on a paced canine tagged MR data set, show sensitivity to abnormal motion caused by pacing. Since all calculation are fast and fully automated, we believe that HARP has great promise for use in a cardiac MRI clinical diagnostic protocol.

Acknowledgments

We thank Dr Elliot McVeigh for providing us with the paced canine MR images. This work was supported by NIH grant R01-HL47405 and nsF grant MIP-9350336.

References

Axel L and Dougherty L 1989 MR imaging of motion with spatial modulation of magnetization *Radiology* **171** 841–5

Beache G M, Wedeen V J, Weisskoff R M, O'Gara P T, Poncelet B P, Chesler D A, Brady T J, Rosen B R and Dinsmore R E 1995 Intramural mechanics in hypertrophic cardiomyopathy: functional mapping with strain-rate MR imaging *Radiology* **197** 117–24

Budinger T F, Berson A, McVeigh E R, Pettigrew R I, Pohost G M, Watson J T and Wickline S A 1998 Cardiac MR imaging: report of a working group sponsored by the national heart, lung, and blood institute *Radiology* **208** 573–6

Constable R T, Rath K M, Sinusas A J and Gore J C 1994 Development and evaluation of tracking algorithms for cardiac wall motion analysis using phase velocity MR imaging *Magn. Res. Med.* **32** 33–42

Fleet D J and Jepson A D 1990 Computation of component image velocity from local phase information *Int. J. Comput. Vision* **5** 77–104

Gurtin M E 1981 *An Introduction to Continuum Mechanics* (New York: Academic)

Marcus J T, Götte M J, Van Rossum A C, Kujer J, Heethaar R M, Axel L and Visser C A 1997 Myocardial function in infarcted and remote regions early after infarction in man: assessment by magnetic resonance tagging and strain analysis *Magn. Res. Med.* **38** 803–10

McVeigh E R, Prinzen F W, Wyman B T, Tsitlik J E, Halperin H R and Hunter W C 1998 Imaging asynchronous mechanical activation of the paced heart with tagged MRI *Magn. Res. Med.* **39** 507–13

Osman N F, Faranesh A, McVeigh E and Prince J L 1999 Tracking cardiac motion using cine harmonic phase (HARP) MRI *Proc. ISMRM 7th Scientific Meeting (22–28 May 1999, Philadelphia)* p 24

Osman N F, Kerwin W S, McVeigh E R and Prince J L 1999a Cardiac motion tracking using CINE harmonic phase (HARP) magnetic resonance imaging *Magn. Reson. Med.* **42** 1048–60

Osman N F, McVeigh E R and Prince J L 2000 Imaging heart motion using harmonic phase MRI *IEEE Trans. Med. Imaging* at press

Osman N F and Prince J L 1998a Direct calculation of 2D components of myocardial strain using sinusoidal MR tagging *Proc. SPIE Med. Imaging Conf. (San Diego)* pp 142–52

——1998b Motion estimation from tagged MR images using angle images *Proc. Int. Conf. Imaging Proc.* vol 1, (Chicago: Computer Society Press) pp 704–8

Pelc N J, Drangova M, Pelc L R, Zhu Y, Noll D C, Bowman B S and Herfkens R J 1995 Tracking of cyclic motion with phase-contrast cine MR velocity data *J. Magn. Res. Imaging* **5** 339–45

Pelc N J, Herfkens R J, Shimakawa A and Enzmann D R 1991 Phase contrast cine magnetic resonance imaging *Magn. Res. Q.* **7** 229–54

Wedeen V J 1992 Magnetic resonance imaging of myocardial kinematics. technique to detect, localize and quantify the strain rates of the active human myocardium *Magn. Res. Med.* **27** 52–67

Wedeen V J, Weisskoff R M, Reese T G, Beache G M, Poncelet B P, Rosen B R and Dinsmore R E 1995 Motionless movies of myocardial strain-rates using stimulated echoes *Magn. Res. Med.* **33** 401–8

Zerhouni E A, Parish D M, Rogers W J, Yang A and Shapiro E P 1988 Human heart: tagging with MR imaging—a method for noninvasive assessment of myocardial motion *Radiology* **169** 59–63